

## Two-dimensional magnetic interactions in LaFeAsO

M. Ramazanoglu,<sup>1,2</sup> J. Lamsal,<sup>1,2</sup> G. S. Tucker,<sup>1,2</sup> J.-Q. Yan,<sup>3</sup> S. Calder,<sup>3</sup> T. Guidi,<sup>4</sup> T. Perring,<sup>4</sup> R. W. McCallum,<sup>1,2</sup>  
T. A. Lograsso,<sup>1,2</sup> A. Kreyssig,<sup>1,2</sup> A. I. Goldman,<sup>1,2</sup> and R. J. McQueeney<sup>1,2</sup>

<sup>1</sup>Ames Laboratory, Ames, Iowa 50011, USA

<sup>2</sup>Department of Physics and Astronomy, Iowa State University, Ames, Iowa 50011, USA

<sup>3</sup>Oak Ridge National Laboratory, Oak Ridge, Tennessee 37831, USA

<sup>4</sup>ISIS Facility, Rutherford Appleton Laboratory, Chilton, Didcot, Oxon OX11 0QX, United Kingdom

(Received 15 March 2013; revised manuscript received 15 April 2013; published 30 April 2013)

Inelastic neutron scattering measurements demonstrate that the magnetic interactions in antiferromagnetic LaFeAsO are two dimensional. Spin-wave velocities within the Fe layer and the magnitude of the spin gap are similar to the  $A\text{Fe}_2\text{As}_2$  based materials. However, the ratio of interlayer and intralayer exchange is found to be less than  $\sim 10^{-4}$  in LaFeAsO, very similar to the cuprates, and  $\sim 100$  times smaller than that found in  $A\text{Fe}_2\text{As}_2$  compounds. The results suggest that the effective dimensionality of the magnetic system is highly variable in the parent compounds of the iron arsenides and weak three-dimensional interactions may limit the maximum attainable superconducting  $T_c$ .

DOI: [10.1103/PhysRevB.87.140509](https://doi.org/10.1103/PhysRevB.87.140509)

PACS number(s): 74.70.Xa, 75.25.-j, 61.05.fg

The discovery of high-temperature superconductivity in the iron arsenide compounds<sup>1</sup> immediately led to comparisons to the copper oxide superconductors. Both systems possess layered crystal structures, suggesting that two-dimensional (2D) behavior may be a shared feature amongst the high-temperature superconductors. In particular, the enhanced spin fluctuations that arise from reduced dimensionality are regarded as a critical element of high-temperature superconductivity. In the case of the copper oxide materials, the magnetism occurs within square copper oxide sheets that are weakly coupled to each other due to separation by ionic layers (such as BaO or LaO). The parent  $\text{La}_2\text{CuO}_4$  compound, for example, is an insulator with a strongly anisotropic resistivity measured within ( $\rho_{ab}$ ) and perpendicular ( $\rho_c$ ) to the Cu layers ( $\rho_c/\rho_{ab} \approx 500$  at high temperatures).<sup>2</sup> The magnetic excitations measured with inelastic neutron scattering (INS) are well understood within a 2D Heisenberg model as the ratio of interlayer to intralayer exchange is very small ( $J_c/J_{ab} \approx 10^{-4}$ – $10^{-5}$ ).<sup>3–5</sup>

In the iron arsenides, magnetism also occurs in well separated square FeAs layers, but the dimensionality of the magnetic interactions is debated. Measurements of the anisotropic properties have been mainly performed on the  $A\text{Fe}_2\text{As}_2$  (122) system ( $A = \text{Ca, Sr, Ba}$ ), where large single crystals are available. In the 122 materials, the FeAs layers are separated by an alkali-earth metal layer (with Fe-Fe layer separation of 5.5–6.5 Å from Ca-Ba, respectively). Transport properties in parent 122 compounds display only a weak anisotropy [for example,  $\rho_c/\rho_{ab} \approx 1$ –3 (Ref. 6)] in contradiction to the strongly 2D transport properties observed in the cuprates. Angle-resolved photoemission (ARPES) experiments on the 122 compounds indicate a significant variation of the Fermi-surface geometry along the  $c$  axis that is also consistent with a three-dimensional (3D) system.<sup>7,8</sup> Finally, INS measurements with  $A = \text{Ca}$  (Refs. 9–11), Sr (Ref. 12), and Ba (Refs. 13 and 14) indicate a fairly substantial interlayer magnetic exchange interaction ( $J_c/J_{ab} \approx 2\%$ – $6\%$ ) which supports three-dimensional magnetism.

Very little is known about the magnetic interactions in the  $R\text{FeAsO}$  (1111) family of superconducting materials that currently claim the largest superconducting transition

temperature of  $T_c^{\text{max}} \approx 55$  K (whereas  $T_c^{\text{max}} \approx 40$  K for the 122 compounds).<sup>15</sup> Based on a larger interlayer spacing ( $\approx 8.7$  Å), 1111 compounds are expected to be closer to the 2D limit than the 122 compounds. The recent availability of large single crystals of LaFeAsO (Ref. 16) have enabled measurements of the anisotropic resistivity ( $\rho_c/\rho_{ab} \approx 2$ – $20$ ),<sup>17</sup> which is similar to the 122 compounds. However, ARPES measurements of the effective dimensionality of the electronic system are inconclusive due to the presence of surface states.<sup>18</sup> In this Rapid Communication, we use INS measurements of the spin-wave spectrum in the parent LaFeAsO compound to show that magnetic exchange coupling is 2D, despite the inference of only weak anisotropy from bulk measurements, with a ratio of exchange interactions comparable to the cuprates ( $J_c/J_{ab} < 10^{-4}$ ). This result provides evidence that the magnetism can vary from 2D to weakly 3D in different iron arsenide compounds, with possible implications for the maximum achievable  $T_c$ .<sup>19</sup>

The sample used for INS experiments consists of dozens of small single crystals of LaFeAsO with a total mass of approximately 600 mg that are coaligned to within  $\sim 2^\circ$ . Details of crystal growth and characterization are described elsewhere.<sup>16</sup> Previous neutron and x-ray scattering measurements show that the crystals undergo a tetragonal-orthorhombic structural phase transition at  $T_S = 155$  K, followed by stripe antiferromagnetic ordering transition at  $T_N = 140$  K.<sup>16</sup> The wave vector of the stripe antiferromagnetic (AFM) ordered state is  $\mathbf{Q}_{\text{AFM}} = (1/2, 1/2, 1/2)_T$  when indexed with reference to the high-temperature  $P4/nmm$  tetragonal structure. In this paper, the scattering data are presented with respect to low-temperature orthorhombic  $Cmma$  unit cell [in other words,  $\mathbf{Q}_{\text{AFM}} = (1, 0, 1/2)_o$ ] where we define  $\mathbf{Q} = (H, K, L) = \frac{2\pi}{a}H\hat{i} + \frac{2\pi}{b}K\hat{j} + \frac{2\pi}{c}L\hat{k}$  and the lattice constants are  $a \approx b = 5.68$  Å and  $c = 8.75$  Å. INS measurements were performed on the MERLIN spectrometer at the ISIS Neutron Scattering Facility at Rutherford-Appleton Laboratory and the HB3 spectrometer at the High Flux Isotope Reactor at Oak Ridge National Laboratory.<sup>20</sup> For these measurements, the samples were mounted in the  $(H, 0, L)$  scattering plane.

For subsequent discussion, both the MERLIN and HB3 data are described using a model of damped Heisenberg spin waves with nearest ( $J_{1a}, J_{1b}$ ) and next-nearest ( $J_2$ ) interactions within the Fe layer, and an interlayer exchange ( $J_c$ ). We also include a single-ion anisotropy energy ( $D$ ) to account for an observed spin gap. Within linear spin-wave theory, the dispersion is given by  $\hbar\omega(\mathbf{q}) = \sqrt{A^2\mathbf{q} - B^2\mathbf{q}}$  with  $A\mathbf{q} = 2S\{D + 2J_2 + J_{1a} + J_c + J_{1b}[\cos(\pi K) - 1]\}$  and  $B\mathbf{q} = 2S[J_{1a}\cos(\pi H) + 2J_2\cos(\pi H)\cos(\pi K) + J_c\cos(2\pi L)]$ . The magnetic susceptibility can be written as a damped simple harmonic oscillator (with damping parameter  $\Gamma$ )

$$\chi''(\mathbf{q}, E) = \frac{\chi_0\Gamma E}{\{E^2 - [\hbar\omega(\mathbf{q})]^2 + \Gamma^2 E^2\}} \quad (1)$$

and the INS intensity in arbitrary units is  $f^2(Q)\chi''(\mathbf{Q} - \mathbf{Q}_{\text{AFM}}, E)(1 - e^{-E/kT})^{-1}$  where  $f(Q)$  is the magnetic form factor of the  $\text{Fe}^{2+}$  ion and  $\mathbf{q} = \mathbf{Q} - \mathbf{Q}_{\text{AFM}}$  is the reduced wave vector within the magnetic Brillouin zone.

MERLIN measurements were performed with the incident neutron beam oriented along  $L$  and an incident energy  $E_i = 150$  meV. The spectrum of spin fluctuations were measured deep in the stripe AFM ordered state at  $T = 5$  K and are shown in Figs. 1(a) and 1(b) for the longitudinal ( $H$ ) and transverse ( $K$ ) directions relative to  $\mathbf{Q}_{\text{AFM}}$  [see Fig. 1(c) for reference].

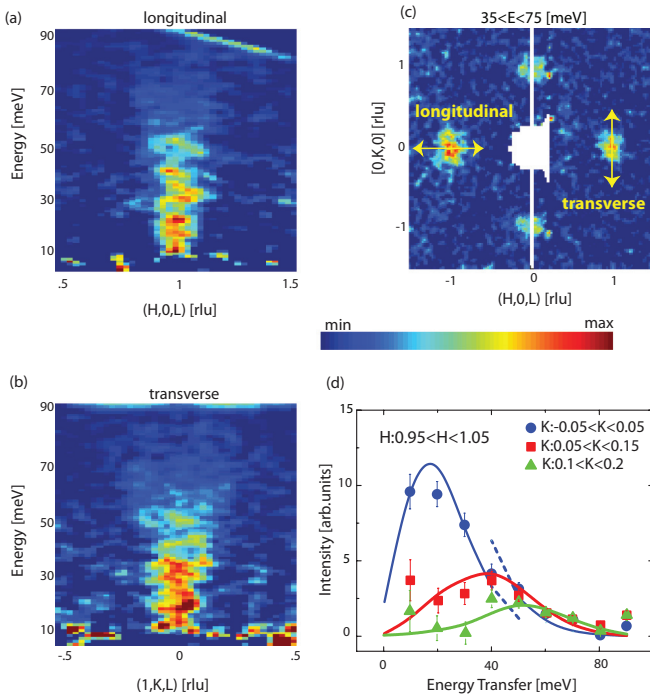


FIG. 1. (Color online) (a) Longitudinal and (b) transverse cuts through the inelastic neutron scattering spectrum of LaFeAsO at  $T = 5$  K as measured on the MERLIN spectrometer with  $E_i = 150$  meV after background subtraction (see text). (c) Data averaged over an energy transfer range from 35–75 meV showing anisotropic spin fluctuations in the  $H$ - $K$  plane centered at  $\mathbf{Q}_{\text{AFM}}$ . (d) Energy spectra at different average  $K$  values along the transverse direction; 0, 0.1, and 0.15. Lines shown are fits described in the text. In these panels, the  $L$  component of the wave vector varies with the in-plane wave vector and energy transfer because of the fixed crystal orientation with respect to the incident beam direction.

In these spectra, an assumed isotropic and energy-dependent nonmagnetic background signal was estimated by summing data at all scattering angles after masking the INS signal near the magnetic zone centers.

The spectrum below 100 meV consists of steep spin waves concentrated close to  $\mathbf{Q}_{\text{AFM}}$  and all symmetrically equivalent wave vectors in the twinned orthorhombic structure [see Fig. 1(c)]. The signal above  $\approx 100$  meV becomes too weak to observe. The MERLIN data are therefore best understood in the small- $q$  limit with spin waves described by an anisotropic linear dispersion relation

$$\hbar\omega(\mathbf{q}) = \sqrt{\Delta_0^2 + v_a^2 q_x^2 + v_b^2 q_y^2 + v_c^2 q_z^2}. \quad (2)$$

The spin-gap and spin-wave velocities are given by  $\Delta_0 = 2S\sqrt{2DJ_+}$ ,  $v_a = aSJ_+$ ,  $v_b = bS\sqrt{J_+J_-}$ ,  $v_c = cS\sqrt{J_cJ_+}$ , respectively, where  $J_+ = 2J_2 + J_{1a} + J_c$  and  $J_- = 2J_2 - J_{1b}$ .

The anisotropy of the dispersion within the Fe layer appears as the elliptical shape of the neutron intensity in Fig. 1(c). Estimates of the longitudinal and transverse spin-wave velocities (based on fits discussed below) are  $v_a = 555 \pm 100$  meV  $\text{\AA}$  and  $v_b = 420 \pm 55$  meV  $\text{\AA}$ , respectively. The in-plane spin-wave velocities in LaFeAsO are comparable, although slightly larger, than the 122 materials, in agreement with first-principles electronic band-structure calculations.<sup>21</sup> The longitudinal velocity exceeds the transverse velocity ( $v_a > v_b$ ) and the anisotropy of the spin excitations within the Fe layer is defined as  $\eta = (v_a^2 - v_b^2)/(v_a^2 + v_b^2)$ .<sup>22</sup> The value of  $\eta = 0.25$  for LaFeAsO is similar to the values found in the parent 122 compounds where  $\eta = 0.2$ –0.4.<sup>22</sup>

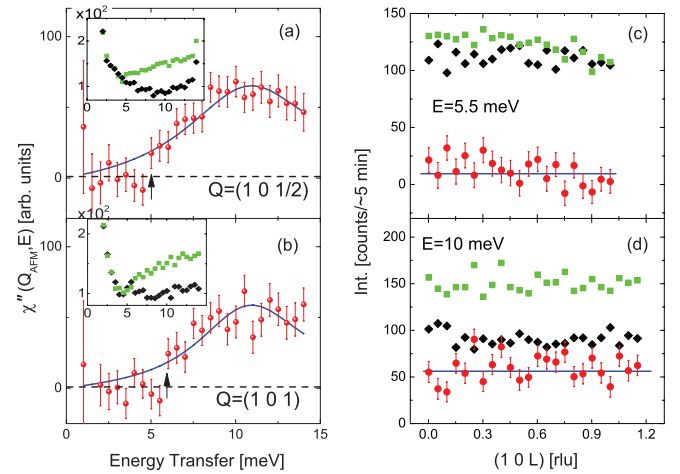


FIG. 2. (Color online) Measurements of the low-energy spin excitations in LaFeAsO at  $T = 5$  K as measured on HB3. Energy dependence of the magnetic scattering at (a)  $\mathbf{Q}_{\text{AFM}} = (1, 0, 1/2)$  and (b) magnetic zone boundary position  $\mathbf{Q}_{\text{ZB}} = (1, 0, 1)$ . Constant energy scans depicting the  $L$  dependence of the magnetic scattering along  $(1, 0, L)$  (c) at gap onset at 5.5 meV, and (d) above the gap at 10 meV. Lines are fits to a damped spin-wave model as described in the text. Panels (c) and (d) and the two insets in panels (a) and (b) show the raw data (green squares) and background scans (crystal rotated from nominal  $\mathbf{Q}$  by  $20^\circ$ , black diamonds) that were used to estimate the magnetic scattering (red symbols) in (a)–(d). The arrows in these panels are indicating the onset value of the energy gap.

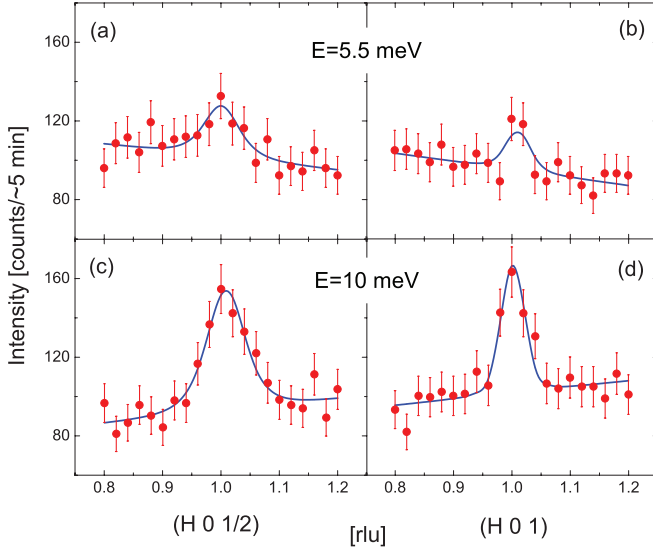


FIG. 3. (Color online) Longitudinal cuts of the low-energy spin excitations in LaFeAsO at  $T = 5$  K as measured on HB3. Data are shown (a) at the onset of the gap at  $E = 5.5$  meV and  $\mathbf{Q}_{\text{AFM}} = (1, 0, 1/2)$ , (b) at 5.5 meV and  $\mathbf{Q}_{\text{ZB}} = (1, 0, 1)$ , (c) at 10 meV and  $\mathbf{Q}_{\text{AFM}}$ , and (d) at 10 meV and  $\mathbf{Q}_{\text{ZB}}$ . Lines show the fits to the damped spin-wave model, described in the text, with only a free amplitude and background. The rest of the parameters are fixed to the values given in Table I. The quality of the agreement between data and the model is also a confirmation of the results.

MERLIN measurements can not ascertain any substantial interlayer exchange interactions, which should appear as  $L$ -dependent oscillations in the intensity. In time-of-flight INS experiments with the  $c$  axis fixed along the incident beam,  $L(E)$  is a function of the energy transfer  $E$ . So, the absence of substantial  $E$ -dependent intensity oscillations in Figs. 1(a), 1(c), and 1(d) indicates 2D magnetism.

In order to verify this 2D behavior, we performed measurements of the low-energy spin excitations at  $T = 5$  K on the same sample using the HB3 spectrometer. Figure 2(a) shows that a substantial spin gap is observed at  $\mathbf{Q}_{\text{AFM}} = (1, 0, 1/2)$ . The gap shows an onset of  $\approx 5$  meV and a peak at  $\approx 11$  meV and is comparable to the spin gaps observed in  $\text{AFe}_2\text{As}_2$  (Refs. 9, 12, 13, and 23) and  $\text{NaFeAs}$  (Ref. 23) compounds. Low-energy INS measurements on polycrystalline LaFeAsO observe a similar-sized spin gap and report a 2D-like response.<sup>24</sup>

The difference between the spin gaps at the magnetic zone center  $\mathbf{Q}_{\text{AFM}}$  ( $\Delta_0$ ) and the magnetic zone boundary point at  $\mathbf{Q}_{\text{ZB}} = (1, 0, 1)$  [ $\mathbf{q}_{\text{ZB}} = (0, 0, 1/2)$ ] provides a direct

TABLE I. Parameters obtained from fitting the  $J_{1a} - J_{1b} - J_2$  spin-wave model with damping and single-ion anisotropy. The damping factor ( $\Gamma$ ), energy gap ( $\Delta_0$ ), and exchange energies ( $\langle SJ_{\pm} \rangle$ ) are in meV while spin-wave velocities  $v_a, v_b$  are in meV  $\text{\AA}$ .

HB3	MERLIN local	MERLIN global
$\Gamma = 8 \pm 1$	$\langle SJ_{+} \rangle = 102 \pm 20$	$\langle SJ_{+} \rangle = 93 \pm 15$
$\Delta_0 = 11.2 \pm 0.6$	$\langle SJ_{-} \rangle = 59 \pm 7$	$\langle SJ_{-} \rangle = 51 \pm 5$
	$\langle v_a \rangle = 555 \pm 100$	
	$\langle v_b \rangle = 420 \pm 55$	

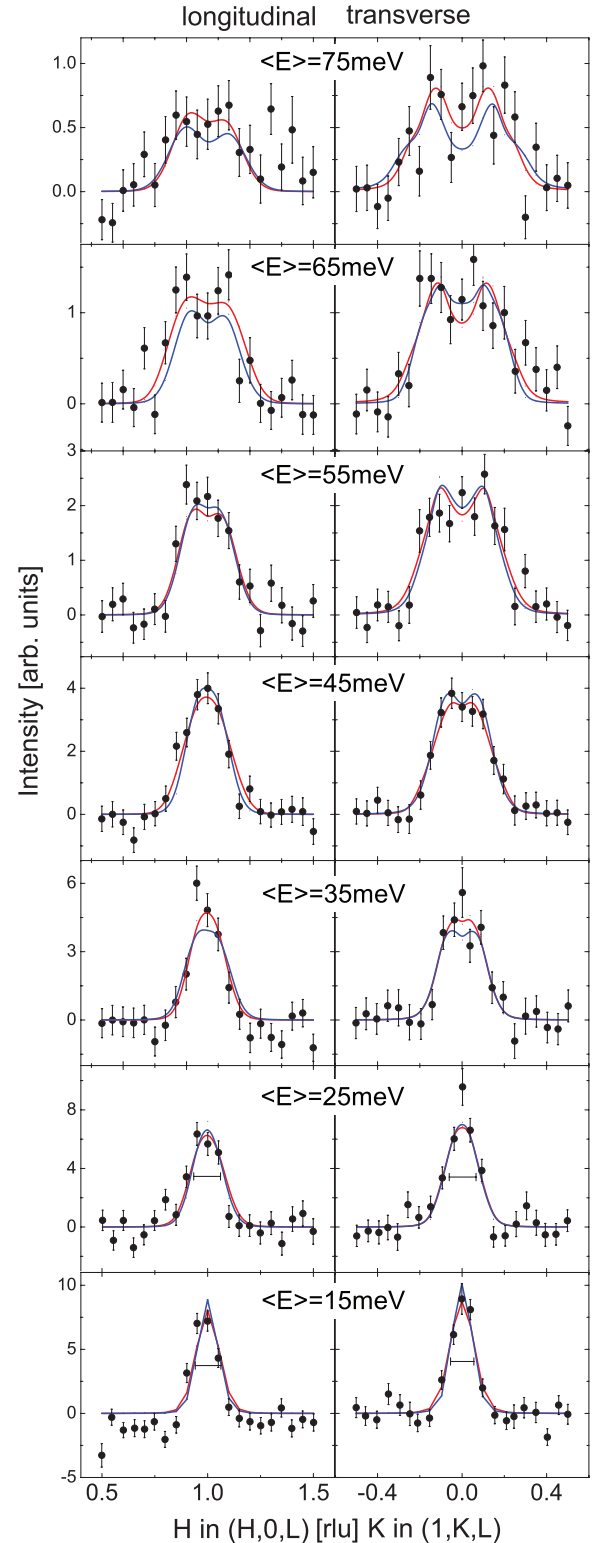


FIG. 4. (Color online) Longitudinal (left) and transverse (right) constant energy cuts of the magnetic scattering in LaFeAsO up to 75 meV as measured on MERLIN. Global (blue line) and local (red line) fits to the damped spin-wave model described in the text are shown. The shoulders in the tails of transverse  $E = 75$  meV cut fit is due to the effect of the twinning of orthorhombic crystal, which is included in the model calculations. For these cuts, the  $L$  component of the wave vector is a function of the in-plane momentum vectors and the energy transfer, as explained earlier.

measurement of  $J_c$ . Using the Heisenberg model, the difference in spin gaps is

$$[\hbar\omega(\mathbf{q}_{\text{ZB}})]^2 - \Delta_0^2 = 16S^2 J_c J_+. \quad (3)$$

A comparison of Figs. 2(a) and 2(b) shows that the magnitude of the spin gap is similar at  $\mathbf{Q}_{\text{ZB}}$ , thereby providing very strong confirmation that  $J_c$  must be weak. Figures 2(c) and 2(d) show an absence of any  $L$ -dependent sinusoidal modulations of the intensity along  $(1,0,L)$  both at the gap onset at 5.5 meV and the peak at 10 meV. Finally, we show in Fig. 3 that a longitudinal cut at the gap onset of 5.5 meV reveals weak intensity at both  $\mathbf{Q}_{\text{AFM}}$  and  $\mathbf{Q}_{\text{ZB}}$ , which again confirms that the two spin gaps are the same. The HB3 data shown in Figs. 2 and 3 was fit using Eqs. (1) and (2) after convolution with the instrumental resolution using the RESLIB program.<sup>25</sup> These data were used to obtain values for the low-energy damping and the spin gaps at  $\mathbf{Q}_{\text{AFM}}$  and  $\mathbf{Q}_{\text{ZB}}$ , yielding  $\Gamma = 8 \pm 1$  meV,  $\Delta_0 = 11.6 \pm 0.5$  meV, and  $\hbar\omega(\mathbf{q}_{\text{ZB}}) = 11.2 \pm 0.5$  meV, respectively. All of these data and subsequent fits give substantive proof that no observable dispersion exists along  $L$  and, therefore, magnetic interactions in LaFeAsO are 2D in nature.

For the MERLIN data, the TOBYFIT program<sup>26</sup> was used to fit the corrected data to the 2D Heisenberg model after convolution with the instrumental resolution and accounting for orthorhombic twinning. The values of  $\Delta_0$  and  $\Gamma$  used in the MERLIN fits are fixed to the values determined by the HB3 data. The corrected data have been symmetrized by averaging all four equivalent quadrants of reciprocal space and subtracting an estimate of the nonmagnetic and background scattering. The main MERLIN fitting results are displayed in Figs. 1 and 4 as a series of longitudinal and transverse cuts through  $\mathbf{Q}_{\text{AFM}}$  at different energy transfers from  $E = 15$  to 75 meV. At low energies, cuts through the steep magnetic excitations consist of a single sharp peak centered at  $\mathbf{Q}_{\text{AFM}}$  due to resolution limitations (the resolution width is indicated by the horizontal line in Fig. 4). Above  $E \sim 55$  meV, the peak splitting from counterpropagating spin-wave modes can be resolved and is more pronounced in transverse cuts where the spin-wave velocity is lower. The two curves in Fig. 4 represent a global fit to all cuts shown (blue line) as well as local fits to each cut (red line) with both procedures yielding similar values for the fitting parameters. Without the ability to observe the spin-wave dispersion at the magnetic zone boundary positions, such as  $\mathbf{q} = (0,1,0)$  [ $\mathbf{Q} = (1,1,0)$ ], the fits are not sensitive to

the difference between nearest-neighbor exchange constants  $S(J_{1a} - J_{1b})$ . The full set of fitting parameters listed in Table I represent both the HB3 and MERLIN data quite well.

In summary, the details of the spin-wave spectrum and magnetic energy scales of LaFeAsO are similar in many ways to the 122 compounds. The energy scale for exchange interactions within the Fe layer and their average in-plane anisotropy are nearly equivalent. This is in accordance with *ab initio* calculations of the spin excitation spectrum.<sup>21</sup> The measurements must be extended up to higher energies in order to determine whether any substantial difference exists between  $J_{1a}$  and  $J_{1b}$ . At lower energies, we find that the magnitude of the spin gap is also similar to the 122 compounds. The common energy scale of the 122 and NaFeAs spin gaps was recently discussed in Ref. 23, as it does not follow from the expectations of simple single-ion anisotropy due to substantial differences in the magnitude of the ordered moments in the two systems. The similar spin gap observed in LaFeAsO, along with its relatively small ordered moment ( $0.4 \mu_B$ ),<sup>27</sup> would seem to add some strength to this argument.

The most important difference in the 122 and 1111 compounds is the interlayer exchange. In our measurements, the zone center and  $(0,0,1/2)$  zone boundary spin gaps in LaFeAsO are equal within error. Considering error bars on the spin-gap magnitudes may allow a 1-meV difference in spin gaps, we can estimate an upper limit for the exchange anisotropy [based on Eq. (3) and the results of the fits to the MERLIN data that determine  $SJ_+$ ] of  $J_c/J_+ < 10^{-4}$  which is similar to the cuprates and places LaFeAsO strongly in the 2D limit. In comparison,  $J_c/J_+ = 2\% - 6\%$  is  $\approx 100$  times larger for the parent 122 compounds.<sup>9-14</sup> The 2D antiferromagnetism found in the 1111 compounds may be responsible for some enhancement of ( $T_c^{\text{max}} \approx 55$  K) and weak 3D magnetic interactions present in the 122 family compounds may present a limitation to higher superconducting transition temperatures ( $T_c^{\text{max}} \approx 40$  K).

R.J.M. would like to thank D. C. Johnston and V. Antropov for useful discussions. The work at Ames Laboratory was supported by the US Department of Energy, Office of Basic Energy Science, Division of Materials Sciences and Engineering under Contract No. DE-AC02-07CH11358. Work at Oak Ridge National Laboratory is supported by US Department of Energy, Office of Basic Energy Sciences, Scientific User Facilities Division.

<sup>1</sup>Y. Kamihara, T. Watanabe, M. Hirano, and H. Hosono, *J. Am. Chem. Soc.* **130**, 3296 (2008).

<sup>2</sup>N. W. Preyer, R. J. Birgeneau, C. Y. Chen, D. R. Gabbe, H. P. Jenssen, M. A. Kastner, P. J. Picone, and Tineke Thio, *Phys. Rev. B* **39**, 11563 (1989).

<sup>3</sup>Y. Endoh, K. Yamada, R. J. Birgeneau, D. R. Gabbe, H. P. Jenssen, M. A. Kastner, C. J. Peters, P. J. Picone, T. R. Thurston, J. M. Tranquada, G. Shirane, Y. Hidaka, M. Oda, Y. Enomoto, M. Suzuki, and T. Murakami, *Phys. Rev. B* **37**, 7443 (1988).

<sup>4</sup>B. Keimer, N. Belk, R. J. Birgeneau, A. Cassanho, C. Y. Chen, M. Greven, M. A. Kastner, A. Aharony, Y. Endoh, R. W. Erwin, and G. Shirane, *Phys. Rev. B* **46**, 14034 (1992).

<sup>5</sup>M. A. Kastner, R. J. Birgeneau, G. Shirane, and Y. Endoh, *Rev. Mod. Phys.* **70**, 897 (1998).

<sup>6</sup>M. A. Tanatar, N. Ni, G. D. Samolyuk, S. L. Budko, P. C. Canfield, and R. Prozorov, *Phys. Rev. B* **79**, 134528 (2009).

<sup>7</sup>A. Heimes, R. Grein, and M. Eschrig, *Phys. Rev. B* **86**, 064528 (2012).

- <sup>8</sup>T. K. Kim, A. N. Yaresko, V. B. Zabolotnyy, A. A. Kordyuk, D. V. Evtushinsky, N. H. Sung, B. K. Cho, T. Samuely, P. Szabo, J. G. Rorigo, J. T. Park, D. S. Inosov, P. Samuely, B. Buchner, and S. V. Borisenko, *Phys. Rev. B* **85**, 014520 (2012).
- <sup>9</sup>R. J. McQueeney, S. O. Diallo, V. P. Antropov, G. D. Samolyuk, C. Broholm, N. Ni, S. Nandi, M. Yethiraj, J. L. Zarestky, J. J. Pulikkotil, A. Kreyssig, M. D. Lumsden, B. N. Harmon, P. C. Canfield, and A. I. Goldman, *Phys. Rev. Lett.* **101**, 227205 (2008).
- <sup>10</sup>S. O. Diallo, V. P. Antropov, T. G. Perring, C. Broholm, J. J. Pulikkotil, N. Ni, S. L. Bud'ko, P. C. Canfield, A. Kreyssig, A. I. Goldman, and R. J. McQueeney, *Phys. Rev. Lett.* **102**, 187206 (2009).
- <sup>11</sup>Jun Zhao, D. T. Adroja, Dao-Xin Yao, R. Bewley, Shiliang Li, X. F. Wang, G. Wu, X. H. Chen, Jiangping Hu, and Pengcheng Dai, *Nat. Phys.* **5**, 555 (2009).
- <sup>12</sup>Jun Zhao, Dao-Xin Yao, Shiliang Li, Tao Hong, Y. Chen, S. Chang, W. Ratcliff Ii, J. W. Lynn, H. A. Mook, G. F. Chen, J. L. Luo, N. L. Wang, E. W. Carlson, Jiangping Hu, and Pengcheng Dai, *Phys. Rev. Lett.* **101**, 167203 (2008).
- <sup>13</sup>K. Matan, R. Morinaga, K. Iida, and T. J. Sato, *Phys. Rev. B* **79**, 054526 (2009).
- <sup>14</sup>L. W. Harriger, H. Q. Luo, M. S. Liu, C. Frost, J. P. Hu, M. R. Norman, and Pengcheng Dai, *Phys. Rev. B* **84**, 054544 (2011).
- <sup>15</sup>D. C. Johnston, *Adv. Phys.* **59**, 803 (2010).
- <sup>16</sup>J. Q. Yan, S. Nandi, J. L. Zarestky, W. Tian, A. Kreyssig, B. Jensen, A. Kracher, K. W. Dennis, R. J. McQueeney, A. I. Goldman, R. W. McCallum, and T. A. Lograsso, *Appl. Phys. Lett.* **95**, 222504 (2009).
- <sup>17</sup>A. Jesche, F. Nitsche, S. Probst, Th Doert, P. Mller, and M. Ruck, *Phys. Rev. B* **86**, 134511 (2012).
- <sup>18</sup>C. Liu *et al.*, *Phys. Rev. B* **82**, 075135 (2010).
- <sup>19</sup>P. Monthoux and G. G. Lonzarich, *Phys. Rev. B* **63**, 054529 (2001).
- <sup>20</sup>HB3 beamline is used with  $E_f = 14.7$  meV (fixed) mode with the collimation of [15 20 20 30].
- <sup>21</sup>Myung Joon Han, Quan Yin, Warren E. Pickett, and Sergey Y. Savrasov, *Phys. Rev. Lett.* **102**, 107003 (2009).
- <sup>22</sup>G. S. Tucker, R. M. Fernandes, H. F. Li, V. Thampy, N. Ni, D. L. Abernathy, S. L. Bud'ko, P. C. Canfield, D. Vaknin, J. Schmalian, and R. J. McQueeney, *Phys. Rev. B* **86**, 024505 (2012).
- <sup>23</sup>J. T. Park, G. Friemel, T. Loew, V. Hinkov, Yuan Li, B. H. Min, D. L. Sun, A. Ivanov, A. Piovano, C. T. Lin, B. Keimer, Y. S. Kwon, and D. S. Inosov, *Phys. Rev. B* **86**, 024437 (2012).
- <sup>24</sup>M. Ishikado *et al.*, *J. Phys. Soc. Jpn.* **78**, 043705 (2009).
- <sup>25</sup>A. Zheludev, [www.neutron.ethz.ch/research/resources/reslib](http://www.neutron.ethz.ch/research/resources/reslib).
- <sup>26</sup>T. G. Perring, <http://tobyfit.isis.rl.ac.uk>.
- <sup>27</sup>Clarina de la Cruz, Q. Huang, J. W. Lynn, Jiying Li, W. Ratcliff Ii, J. L. Zarestky, H. A. Mook, G. F. Chen, J. L. Luo, N. L. Wang, and Pengcheng Dai, *Nature (London)* **453**, 899 (2008).